Surface proton transport of fully protonated poly(aspartic acid) thin films on quartz substrates

Yuki Nagao*, Takahiro Kubo

School of Materials Science, Japan Advanced Institute of Science and Technology, 1-1 Asahidai, Nomi, Ishikawa 923-1292, Japan

Corresponding author: ynagao@jaist.ac.jp, +81(Japan)-761-51-1541

Abstract

Thin film structure and the proton transport property of fully protonated poly(aspartic acid) (P-Asp100) have been investigated. An earlier study assessed partially protonated poly(aspartic acid), highly oriented thin film structure and enhancement of the internal proton transport. In this study of P-Asp100, IR *p*-polarized multiple-angle incidence resolution (P-MAIR) spectra were measured to investigate the thin film structure. The obtained thin films, with thicknesses of 120 nm to 670 nm, had no oriented structure. Relative humidity dependence of the resistance, proton conductivity, and normalized resistance were examined to ascertain the proton transport property of P-Asp100 thin

films. The obtained data showed that the proton transport of P-Asp100 thin films might occur on the surface, not inside of the thin film. This phenomenon might be related with the proton transport of the biological system.

Keywords

Proton conduction, Surface conduction, Polypeptide, Bacteriorhodopsin

1. Introduction

In biological systems, proton transfer in protein ionic channels has attracted many researchers since the 1960s [1]. Many have investigated the purple membrane including bacteriorhodopsin for its fundamental role in proton transport in biological systems [2–11]. Surface proton conduction at the lipid monolayer has also been studied intensively [12-18]. Reportedly, 20-times enhancement of proton diffusion on the surface was achieved compared to bulk water [12], but other researchers strongly disputed the contents of that report [13]. Nevertheless, enhancement of ionic transport at the interface still attracts many researchers of surface science and ionics.

Regarding work in the solid state ionics research field, Liang reported approximately 50-times enhancement of Li^+ ion conduction in 1973 [19]. The sample was simply mixed with inert Al_2O_3 ultrafine particles into LiI. However, ionic conductivity depends strongly on the contents of Al_2O_3 ultrafine particles. In most cases, when enhancement was observed, the second phase consisted of a nonconducting material such as SiO_2 or Al_2O_3, which is nearly insoluble in the host material. This finding gave us the opportunity to improve the ionic transport property by the inorganic–organic hybrid system. Recently many hybrid materials have been reported for proton conductors with consideration of the p*K*a difference between the proton

donor and acceptor.

Many acid–base combinations of proton conductors have been reported for improving proton transport and stability or for anhydrous proton conduction [20–23]. The p*K*a difference between the acidic and basic property of materials was applied for the proton transport system based on the concept of a proton donor and acceptor. Another familiar proton transfer with the p*K*a difference is apparent in the biological system: bacteriorhodopsin. It pumps protons from the cell interior to the external medium when the light is irradiated. The retinal in bacteriorhodopsin receives light for the activation. Then it changes the p*K*a-correspondent amino acid residues step-by-step around the retinal. The aspartic acid residue in bacteriorhodopsin polypeptides plays a crucial role in proton transport [2,7].

Recently, we have found markedly high proton conductivity in the thin films of partially protonated poly(aspartic acid) on quartz substrates [24]. This thin film exhibited highly molecular orientation spontaneously. The wavenumber of the IR spectrum suggests that this thin film has non-periodic secondary structures, e.g., β-turn [25] and α-sheet [26] structures. The proton conductivity of the thin film was one order of magnitude higher than the random oriented specimen. Results suggest that the origin for the proton conductivity enhancement is attributable to the oriented structural effects.

However, a study of this enhancement of the proton transport using poly(aspartic acid) itself is insufficient to understand this phenomenon. In this study, fully protonated poly(aspartic acid) (P-Asp100) was synthesized to investigate the proton transport properties of thin films. Although P-Asp100 has movable protons at the side chain, protons are not easily released and are hard to move to the next proton site in P-Asp100 because of the weak acid p*K*a and fully protonated state. Therefore we speculated that the results obtained in the case of P-Asp100 would differ from those of the partially protonated poly(aspartic acid).

2. Experimental

Fully protonated P-Asp100 was synthesized according to Scheme 1. D, L-aspartic acid, o-phosphoric acid, methanol, sodium hydroxide, and HCl were purchased from Wako Pure Chemical Industries Ltd. D, L-Aspartic acid of 5 g and 85% o-phosphoric acid of 3 ml were added to a 100 ml round-bottom flask and were mixed for 10 min under Ar atmosphere. The mixture was heated at 170°C for 16 hr. The product was washed with methanol and water. The residue was washed with methanol and dried under reduced pressure. The dried sample of 3.6 g and a solution of sodium hydroxide of 1.5 g with 15 ml of deionized water were added to a 200 ml beaker with stirring for

20 min. A white precipitate was obtained by adding methanol of 100 ml. The sample was washed with methanol and was separated from the supernatant, in which the centrifuge technique was used in washing and separation procedures. The obtained sample was dried under reduced pressure. For protonation, the sample was dissolved completely in distilled water. Then an ion exchange process was performed using Amberlyst. Using a rotary vacuum evaporator, the protonated sample was obtained and dried under vacuum. In fact, 100% of protonation was confirmed using the titration method. The obtained sample (P-Asp100) was characterized via ^{1}H NMR (Avance III; Bruker BioSpin Inc.) and FT-IR measurements using an ATR accessory (Nicolet 6700; Thermo Fisher Scientific Inc.). Gel permeation chromatography (ChromNAV-GPC; Jasco Corp.) showed the average molecular weight as ca. 6500, as determined.

The P-Asp100 thin films were prepared by spin coating using a spincoater (ACT-200; Active) on mirror-polished quartz substrates or Si wafer. The quartz substrate and Si wafer size were, respectively, 17 mmϕ × 1 mm and 20 × 30 × 0.5 mm. Before film deposition, each substrate was subjected to several cleaning processes. Then plasma treatment was performed using a vacuum plasma system (Cute-MP; Femto Science) to improve surface hydrophilicity. The thickness was determined using a contact stylus profiler (P-10; KLA Tencor Corp.). The roughness measurement showed

that its smoothness was sufficient for IR measurement and impedance analysis.

For *p*-polarized multiple-angle incidence resolution (p-MAIR) spectroscopy [27–30], measurements were taken using a FT-IR spectrometer (Nicolet 6700; Thermo Fisher Scientific Inc.) equipped with a mercury–cadmium–telluride (MCT) detector. A mirror-polished Si wafer was used for p-MAIR measurements. Single-beam spectra were collected from 38° to 8° at 6° steps between the angle of incidence. The aperture was fully opened (size of 150) and a metal plate with small pores was placed in the light path of the incident beam to prevent saturation. To obtain p-polarized light, a ZnSe polarizer was used. The cleaned Si wafer was used to obtain reference data.

For impedance measurements, the thin films were measured in relative humidity (RH) of 70–90% using an impedance/gain-phase analyzer (SI1260; Solartron Analytical) and a dielectric interface system (1296; Solartron Analytical). The RH and temperature were controlled using a humidity-controlled and temperature-controlled chamber (SH-221; Espec Corp.). The temperature was set at 298 K. The thin films were prepared by spincoating on the quartz substrate. The thin film size was ca. 5×10 mm. The electrode configuration was selected to obtain measurements of the current flow in the plane parallel to the substrate surface. The electrode was located at the edge of the film, with a parallel electrode configuration. Porous gold paint (SILBEST No. 8560;

Tokuriki Chemical Research) was used for electrodes and was covered at the side of the film. The inter-electrode distance was ca. 4.0 mm.

3. Results and Discussion

3.1 Characterization of P-Asp100

Figure 1 shows the ^{1}H NMR spectrum for P-Asp100. DMSO-d_6 was used for the solvent. The peaks at 4.5 and 2.6 ppm are attributed respectively to the CH and CH_2 groups. The peaks at 8.1 and 12.5 ppm respectively correspond to the protons of NH and COOH groups. Scheme 1 shows that integration of proton peaks in ^{1}H NMR spectrum produces good agreement with the number of protons.

Figure 2 shows the ATR spectrum for P-Asp100. The amide I (CO of amide group) and amide II (NH of amide group) bands appeared respectively at 1650 and 1530 cm^{-1}. The wavenumbers of these bands are almost identical values to those of the partially protonated poly(aspartic acid) [24]. The new band at 1730 cm^{-1} corresponds to the CO vibration mode of COOH at the side chain. Absorption around 1600 cm^{-1} derived from the deprotonated COO^- group was not observed because P-Asp had no COO^- group.

3.2 Thin film structure

In an earlier study of the partially protonated poly(aspartic acid) thin film, thin films were prepared on the MgO substrate [24]. In this study, the proton transport property was investigated with the quartz substrates. Therefore for the measurement of p-MAIRS, as-received Si wafer was used without removing the oxidized surface. The obtained thickness of the thin films was 120–670 nm. Figure 3(a) shows p-MAIR spectra for the 120 nm thick P-Asp100 thin film on the Si wafer. Absorption around 1600 cm^{-1} derived from the deprotonated COO^- group was not observed. This result is consistent to obtain fully protonated P-Asp100. In the in-plane mode, the amide I and amide II bands were observed, respectively, at 1655 and 1530 cm^{-1}. The in-plane spectrum was similar with the ATR spectrum in Fig. 2. However, in the out-of-plane spectrum, all peaks were shifted to the higher wavenumber. The amide I and amide II bands in the out-of-plane were observed, respectively, at 1667 and 1539 cm^{-1}. The CO mode of the COOH groups was also shifted respectively from 1730 to 1742 cm^{-1}. The reason for these shifts has not been revealed. In a previous study with the partially protonated poly(aspartic acid) thin film, the shapes of spectra between those in-plane and out-of-plane differed greatly. The amide groups had a highly oriented structure [24]. However, spectra with fully protonated P-Asp100 thin film were found to be similar excluding the peak shift between the in-plane and out-of-plane spectra in this study. The

degree of the orientation was calculated using the following eq. (1) [31].

$$\varphi = \tan^{-1}\sqrt{\frac{2A_{IP}}{A_{OP}}} \quad (1)$$

Therein, φ is the orientation angle from normal to the surface; A_{IP} and A_{OP} respectively stand for band intensities of identical bands in the in-plane and out-of-plane spectra. The respective degrees of orientation for the amide I and amide II bands were 52° and 56°. These angles were close to the 54.7°, the so-called magic angle [32]. The amide I and amide II groups correspond to a disordered state. For COOH groups at the side chain, the degree of the orientation was 48°. The value was lower than that of the magic angle. This result suggests that the COOH group had an oriented state.

To confirm the thin film structure changes that occur with the thickness, Figs. 3(b), 3(c), and 3(d) show p-MAIR spectra with thicknesses of 300, 590 and 670 nm. Along with the thickness, the band intensity of COOH group increased slightly compared to that of amide I. Table 1 presents the wavenumber for each in-plane and out-of-plane band. No thickness dependence was observed in this thickness range, but all wavenumbers of the out-of-plane spectrum were shifted to a higher wavenumber than those of the in-plane spectrum. Table 2 presents the degree of orientation for each assigned band calculated using eq. (1). As a trend, the degree of the orientation decreased with thickness, but no large structural change was observed for 120–670 nm

thickness. The thin film structure does not change drastically with thickness in P-Asp100.

Figure 4 shows the RH-dependent ATR measurements for the 120-nm-thick P-Asp100 thin film. These measurements were conducted at 50%, 70%, and 90% RH with the time interval of 30 min for every 20% RH increment. Before each measurement, the sample was maintained at 298 K and under the specified humidity condition for 30 min. Each measurement was performed within 10 s of the sample being removed from the humidity chamber. The band intensity of the COOH group and amide I increased slightly with RH. The thin film adsorbs water molecules with the RH. Presumably, the adsorption of the water molecules can contribute to increased band intensity of COOH group and amide I.

3.3 Proton transport property

Typical complex impedance plots of the P-Asp100 thin film with 600-nm-thick at 70% RH are presented in Fig. 5. The impedance was obtained from the semicircle diameter. The obtained resistance was 6×10^{10} Ω. Figure 6 shows the relative humidity dependence of the resistance. The dependence was investigated using three thin films with respective thicknesses of 100 nm, 320 nm, and 600 nm. The Log (resistance)

depended strongly on the relative humidity. Furthermore, the relation was linear. The difference of the resistance between 70–90% RH was greater than three orders of magnitude. Presumably, this large difference was derived from the water uptake in the thin films. No thickness dependence of the resistance was observed. In the typical case, the resistance is expected to depend on the thickness. Therefore, the following two methods were considered for the discussion. One is an internal proton transport in P-Asp100 thin film as proton conduction. Another is a surface proton transport as surface conduction. Thin-film conductivity (σ) was estimated as

$$\sigma = \frac{d}{Rlt} \tag{2}$$

where d stands for the distance between the gold electrodes, R signifies the resistance value obtained directly from the impedance measurement, l denotes the length of the contact electrodes, and t represents the film thickness. Figure 7 shows the RH dependence of the proton conductivity. The conductivity depends on both RH and thickness. The conductivity increased concomitantly with decreasing thickness. In the typical case, the conductivity is independent of the thickness. When the conductivity depends on the thickness, one must consider the surface effect for enhanced conduction [33–36]. Therefore the normalized resistance (R') was also calculated using the following equation to investigate the possibility of the surface conduction.

$$R' = \frac{Rl}{d} \quad (3)$$

Figure 8 shows the RH dependence of the normalized resistance. The normalized resistance did not depend on the thickness. It gave an almost constant value. If the internal conduction occurred in the thin film, then the normalized resistance depends on the thickness. It is therefore likely that the P-Asp100 thin film has ~~only~~ surface conduction. Few reports describe the surface proton transport in synthesized polymer thin films. In a previous study, the partially protonated poly(aspartic acid) exhibited internal proton conduction [24]. As one possibility explaining the reason for surface transport, the structure was completely different between P-Asp100 and the partially protonated poly(aspartic acid) thin films. In fact, the partially protonated P-Asp thin film had an oriented structure. This oriented structure was more ordered than that of P-Asp100 thin film. A proton might be mobile into the inside of the thin film. However, the P-Asp100 thin film was not oriented. Therefore, protons might have difficulty moving to the inside of the thin film rather than to the surface. Another contribution for the surface transport is derived from the weak acid p*K*a. Protons exist at the COOH groups of the side chain. This proton exhibits a weak acid p*K*a. If the proton is fully charged in P-Asp100 based on the weak acid property, then proton is not released easily from the acidic site of the COOH group.

In summary, the thin film structure of the fully protonated P-Asp100 was found to differ greatly from that of the partially protonated poly(aspartic acid). In an earlier study, the thin film of the partially protonated poly(aspartic acid) exhibited highly internal proton transport. However, in this study, dominant proton transport would occur on the surface of the thin film, not inside of the film. This difference of the proton transport can derive from two reasons: the different structure and the characteristic property of the weak acid p*K*a. In P-Asp100, the COOH groups play a role as the proton donor. The system has no proton acceptor. It is necessary to consider the balance of p*K*a when treating the weak acid system. This result could contribute to understand the proton transport in biological systems.

4. Conclusion

Fundamental proton transport in a purple membrane has been investigated since the 1970s, the aspartic acid residue plays a crucial role in proton transport. The conformation change of the aspartic acid residues provides an opportunity for changing p*K*a. Therefore, it partially plays a role in pumping protons from the cell interior to the external medium proton pump. In our previous study of the partially protonated

poly(aspartic acid), a highly oriented thin film structure and enhancement of the internal proton transport were observed. In this study, to elucidate the proton transport property of the poly(aspartic acid) further, the proton transport property of the fully protonated poly(aspartic acid) (P-Asp100) was investigated. Judging from the obtained data, the proton transport of P-Asp100 thin films might occur on the surface, not inside of the thin film. This result differs greatly in the case of the partially protonated poly(aspartic acid). This difference in proton transport can derive from the different structure or from the characteristic property of the weak acid p*K*a. In P-Asp100, the fully protonated COOH groups play a role only as a proton donor, with no proton acceptor in the system. Therefore protons can not be released easily with mobility into the thin film. It is necessary to consider a balance of p*K*a when treating a weak acid system. This result is expected to contribute to the elucidation of proton transport in biological systems.

Acknowledgments

This work was supported financially by the Japan Society for the Promotion of Science (JSPS) through the Funding Program (GR060) for Next Generation World-Leading Researchers (NEXT Program), initiated by the Council for Science and Technology Policy (CSTP). This work was partially supported by the Ogasawara

Foundation for the Promotion of Science and Engineering.

References

[1] P. Mitchell, Coupling of phosphorylation to electron and hydrogen transfer by a chemi-osmotic type of mechanism, Nature, 191 (1961) 144-148.

[2] H.J. Butt, K. Fendler, E. Bamberg, J. Tittor, D. Oesterhelt, Aspartic acids 96 and 85 play a central role in the function of bacteriorhodopsin as a proton pump, EMBO J., 8 (1989) 1657-1663.

[3] A. Der, S. Szaraz, R. Toth-Boconadi, Z. Tokaji, L. Keszthelyi, W. Stoeckenius, Alternative translocation of protons and halide ions by bacteriorhodopsin, Proc. Natl. Acad. Sci. U. S. A., 88 (1991) 4751-4755.

[4] S. Krimm, A.M. Dwivedi, Infrared spectrum of the purple membrane: clue to a proton conduction mechanism?, Science, 216 (1982) 407-408.

[5] R.H. Lozier, R.A. Bogomolni, W. Stoeckenius, a light-driven proton pump in Halobacterium halobium, Biophys. J., 15 (1975) 955-962.

[6] E. Nachliel, M. Gutman, S. Kiryati, N.A. Dencher, Protonation dynamics of the extracellular and cytoplasmic surface of bacteriorhodopsin in the purple membrane, Proc. Natl. Acad. Sci. U. S. A., 93 (1996) 10747-10752.

[7] R. Needleman, M. Chang, B. Ni, G. Varo, J. Fornes, S.H. White, J.K. Lanyi, Properties of Asp212----Asn bacteriorhodopsin suggest that Asp212 and Asp85 both

participate in a counterion and proton acceptor complex near the Schiff base, J. Biol. Chem., 266 (1991) 11478-11484.

[8] E. Racker, W. Stoeckenius, Reconstitution of purple membrane vesicles catalyzing light-driven proton uptake and adenosine triphosphate formation, J. Biol. Chem., 249 (1974) 662-663.

[9] J. Tittor, U. Schweiger, D. Oesterhelt, E. Bamberg, Inversion of proton translocation in bacteriorhodopsin mutants D85N, D85T, and D85,96N, Biophys. J., 67 (1994) 1682-1690.

[10] H.W. Trissl, Photochem. Photoelectric measurements of purple membranes, Photochem. Photobiol., 51 (1990) 793-818.

[11] G. Varo, L. Keszthelyi, Photoelectric signals from dried oriented purple membranes of Halobacterium halobium, Biophys. J., 43 (1983) 47-51.

[12] J. Teissie, M. Prats, P. Soucaille, J.F. Tocanne, Evidence for conduction of protons along the interface between water and a polar lipid monolayer, Proc. Natl. Acad. Sci. U. S. A., 82 (1985) 3217-3221.

[13] A. Polle, W. Junge, Proton diffusion along the membrane surface of thylakoids is not enhanced over that in bulk water, Biophys. J., 56 (1989) 27-31.

[14] M. Prats, J.F. Tocanne, J. Teissie, Lateral diffusion of protons along phospholipid

monolayers, J. Membr. Biol., 99 (1987) 225-227.

[15] J. Kasianowicz, R. Benz, M. Gutman, S. McLaughlin, Reply to: Lateral diffusion of protons along phospholipid monolayers, J. Membr. Biol., 99 (1987) 227.

[16] H. Morgan, D.M. Taylor, O.N. Oliveira, Proton transport at the monolayer-water Interface, Biochim. Biophys. Acta, 1062 (1991) 149-156.

[17] I. Sakurai, Y. Kawamura, Lateral electrical conduction along a phosphatidylcholine monolayer, Biochim. Biophys. Acta, 904 (1987) 405-409.

[18] K. Leberle, I. Kempf, G. Zundel, An intramolecular hydrogen bond with large proton polarizability within the head group of phosphatidylserine. An infrared investigation, Biophys. J., 55 (1989) 637-648.

[19] C.C. Liang, Conduction characteristics of the lithium iodide-aluminum oxide solid electrolytes, J. Electrochem. Soc., 120 (1973) 1289-1292.

[20] T.L. Greaves, C.J. Drummond, Protic ionic liquids: Properties and applications, Chem. Rev., 108 (2008) 206-237.

[21] Q.F. Li, J.O. Jensen, R.F. Savinell, N.J. Bjerrum, High temperature proton exchange membranes based on polybenzimidazoles for fuel cells, Prog. Polym. Sci., 34 (2009) 449-477.

[22] C. Yang, P. Costamagna, S. Srinivasan, J. Benziger, A.B. Bocarsly, Approaches and

technical challenges to high temperature operation of proton exchange membrane fuel cells, J. Power Sources, 103 (2001) 1-9.

[23] K.D. Kreuer, On the development of proton conducting polymer membranes for hydrogen and methanol fuel cells, J. Membr. Sci., 185 (2001) 29-39.

[24] Y. Nagao, J. Matsui, T. Abe, H. Hiramatsu, H. Yamamoto, T. Miyashita, N. Sata, H. Yugami, Enhancement of proton transport in an oriented polypeptide thin film, Langmuir, 29 (2013) 6798-6804.

[25] S. Krimm, J. Bandekar, Vibrational spectroscopy and conformation of peptides, polypeptides, and proteins, Adv. Protein Chem., 38 (1986) 181-364.

[26] H. Torii, Amide I infrared spectral features characteristic of some untypical conformations appearing in the structures suggested for amyloids, J. Phys. Chem. B, 112 (2008) 8737-8743.

[27] T. Hasegawa, A novel measurement technique of pure out-of-plane vibrational modes in thin films on a nonmetallic material with no polarizer, J. Phys. Chem. B, 106 (2002) 4112-4115.

[28] T. Hasegawa, Y. Itoh, A. Kasuya, Experimental optimization of p-polarized MAIR spectrometry performed on a fourier transform infrared spectrometer, Anal. Sci., 24 (2008) 105-109.

[29] T. Hasegawa, L. Matsumoto, S. Kitamura, S. Amino, S. Katada, J. Nishijo, Optimum condition of Fourier transform infrared multiple-angle incidence resolution spectrometry for surface analysis, Anal. Chem., 74 (2002) 6049-6054.

[30] T. Hasegawa, Advanced multiple-angle incidence resolution spectrometry for thin-layer analysis on a low-refractive-index substrate, Anal. Chem., 79 (2007) 4385-4389.

[31] M. Matsunaga, T. Suzuki, K. Yamamoto, T. Hasegawa, Molecular structure analysis in a dip-coated thin film of poly (2-perfluorooctylethyl acrylate) by infrared multiple-angle incidence resolution spectrometry, Macromolecules, 41 (2008) 5780-5784.

[32] T. Hasegawa, S. Takeda, A. Kawaguchi, J. Umemura, Quantitative-analysis of uniaxial molecular-orientation in Lamgmuir-Blodgett-films by infrared reflection spectroscopy, Langmuir, 11 (1995) 1236-1243.

[33] J. Maier, Defect chemistry and ionic conductivity in thin films, Solid State Ionics, 23 (1987) 59-67.

[34] J. Maier, Ionic conduction in space charge regions, Prog. Solid State Chem., 23 (1995) 171-263.

[35] J. Schoonman, Nanoionics, Solid State Ionics, 157 (2003) 319-326.

[36] J. Maier, Nanoionics: Ion transport and electrochemical storage in confined systems, Nat. Mater., 4 (2005) 805-815.

Scheme and Figure captions

Scheme 1 Synthesis of fully protonated poly(aspartic acid) (P-Asp100).

Figure 1 ^{1}H NMR spectrum for P-Asp100.

Figure 2 IR spectrum by ATR method for P-Asp100.

Figure 3 p-MAIR spectra for P-Asp thin films with different thicknesses: (a) 120 nm, (b) 300 nm, (c) 590 nm, and (d) 670 nm. The IP component has two orthogonal directions of the electric field. Therefore, the IP absorbance was multiplied by a factor of 2 [27].

Figure 4 IR spectra with different humidity conditions by ATR methods. Dotted line is under 50% RH. Dashed line is under 70% RH. Solid line is under 90% RH.

Figure 5 Typical impedance plots for P-Asp100 thin film with 600 nm thick under 70% RH and 298 K.

Figure 6 Relative humidity dependence of resistivity for P-Asp100 thin films: □, 100 nm thick; ○, 320 nm thick; ♦, 600 nm thick.

Figure 7 Relative humidity dependence of proton conductivity for P-Asp100 thin films: □, 100 nm thick; ○, 320 nm thick; ♦, 600 nm thick. These are invalid data. See 3.3 Proton transport property.

Figure 8 Relative humidity dependence of the surface resistance for P-Asp100 thin

films: □, 100 nm thick; ○, 320 nm thick; ♦, 600 nm thick.

Table captions

Table 1 Summarized IP and OP wavenumber position of CO mode of COOH groups, amide I and amide II with each thickness

Table 2 Summarized degree of orientation for the CO mode of COOH groups, amide I, amide II, and CN mode with each thickness

Table 1

Thickness / nm	IP_{COOH} / cm^{-1}	OP_{COOH} / cm^{-1}	IP_{amideI} / cm^{-1}	OP_{amideI} / cm^{-1}	$IP_{amideII}$ / cm^{-1}	$OP_{amideII}$ / cm^{-1}
120	1730	1742	1655	1667	1530	1539
300	1730	1740	1657	1667	1533	1536
590	1733	1739	1660	1667	1535	1538
670	1735	1740	1660	1665	1533	1539

Table 2

Thickness	φ_{COOH}	φ_{amideI}	$\varphi_{amideII}$	φ_{CN}
120 nm	48°	52°	56°	57°
300 nm	47°	51°	54°	57°
590 nm	47°	49°	53°	56°
670 nm	47°	49°	52°	54°

Scheme 1

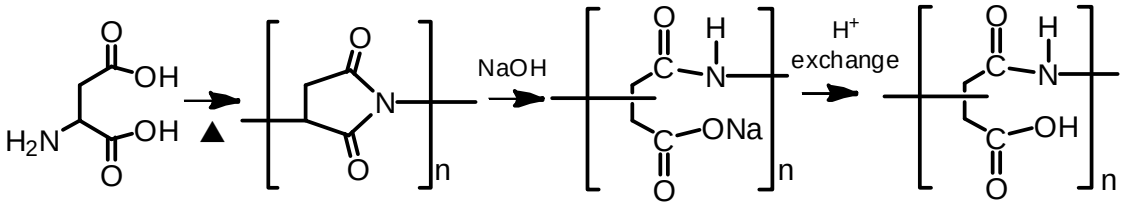
NaOH
H+
exchange
D, L-aspartic acid
Asp
Polysuccinimide
PSI
Sodium polyaspartate
Poly(aspartic acid)
P-Asp100

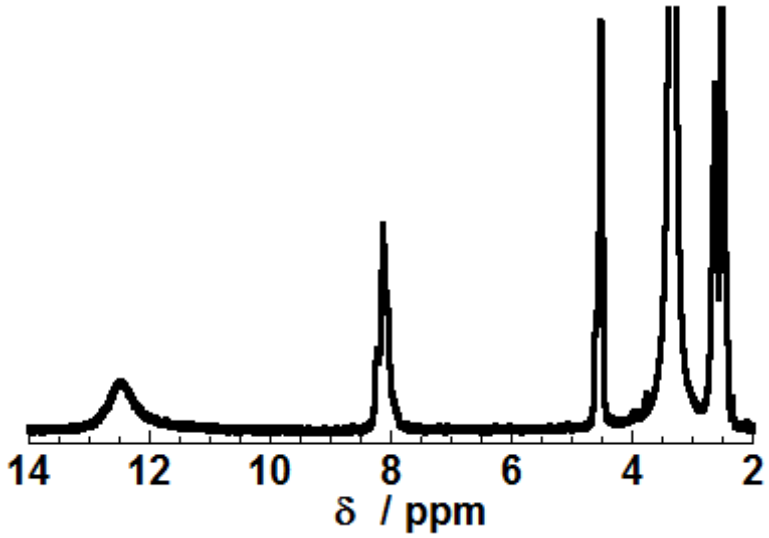

Fig. 1

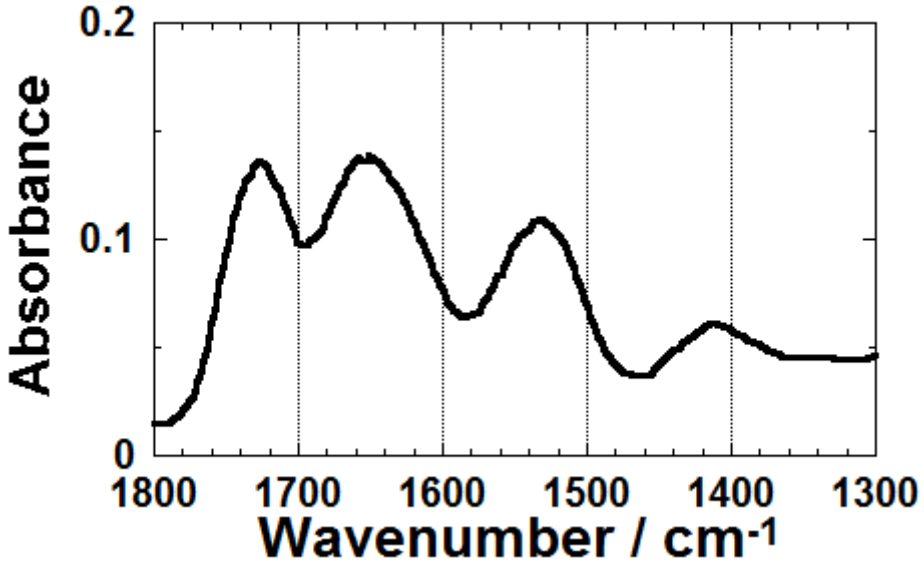
0.2
0.1
0
Absorbance
1800
1700
1600
1500
1400
1300
Wavenumber / cm-1

Fig. 2

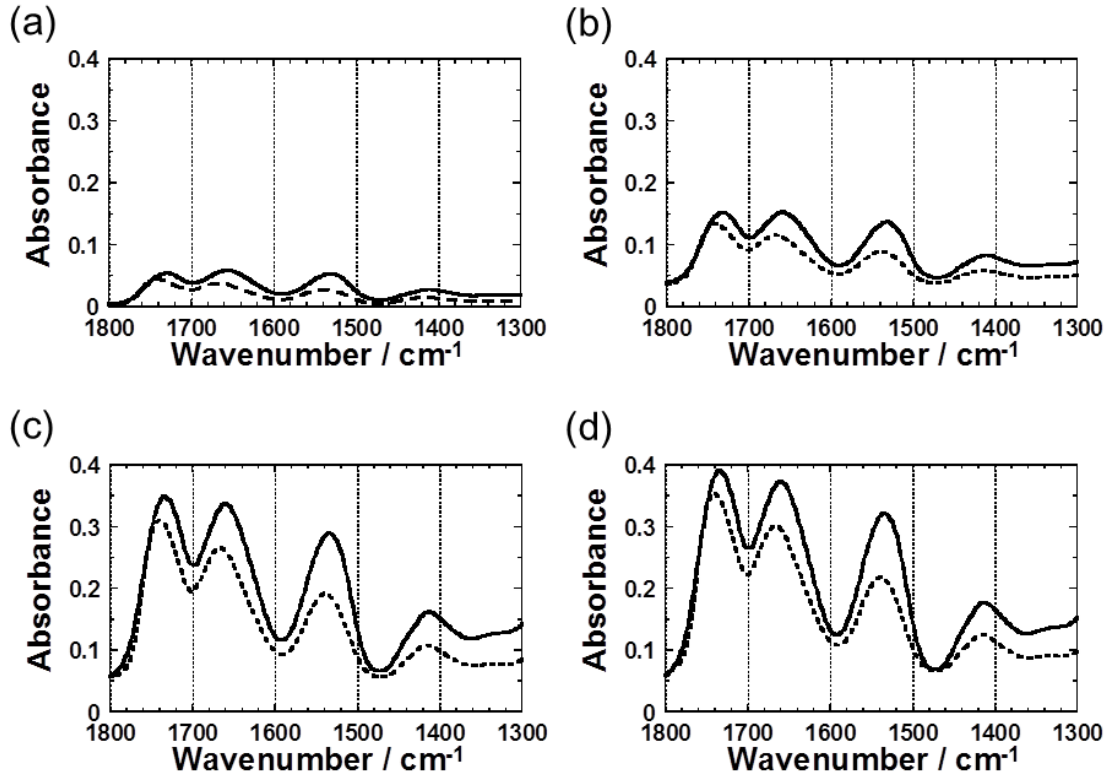
(a)
(b)
(c)
(d)
Absorbance
Wavenumber / cm-1
0.4
0.3
0.2
0.1
0
1800
1700
1600
1500
1400
1300

Fig. 3

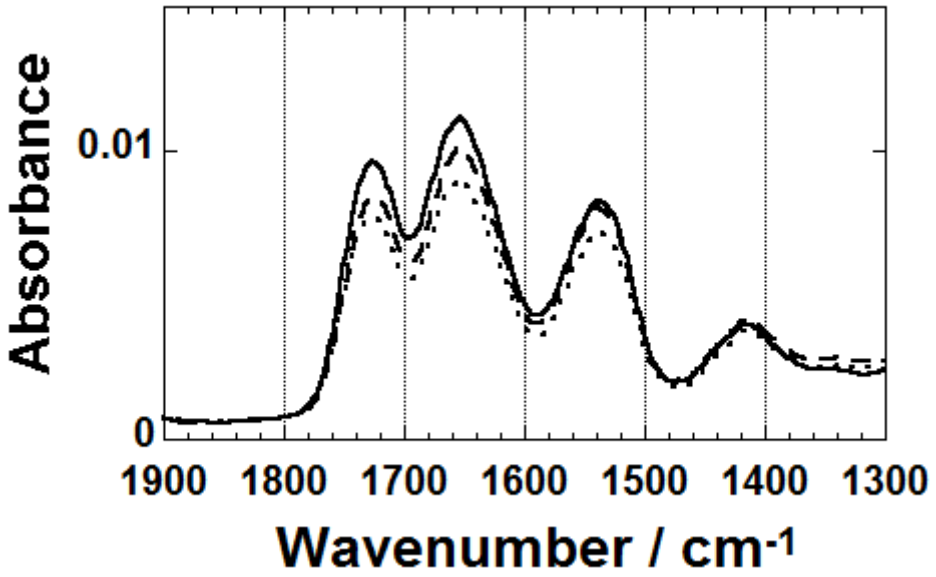
Absorbance
0.01
0
1900
1800
1700
1600
1500
1400
1300
Wavenumber / cm-1

Fig. 4

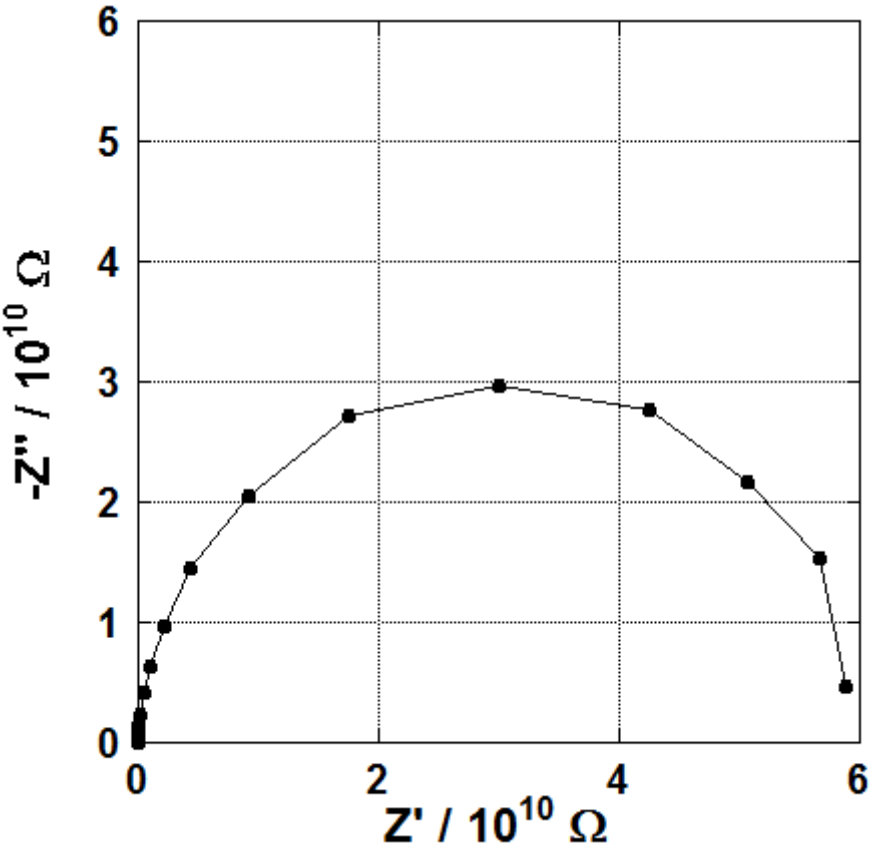

Fig. 5

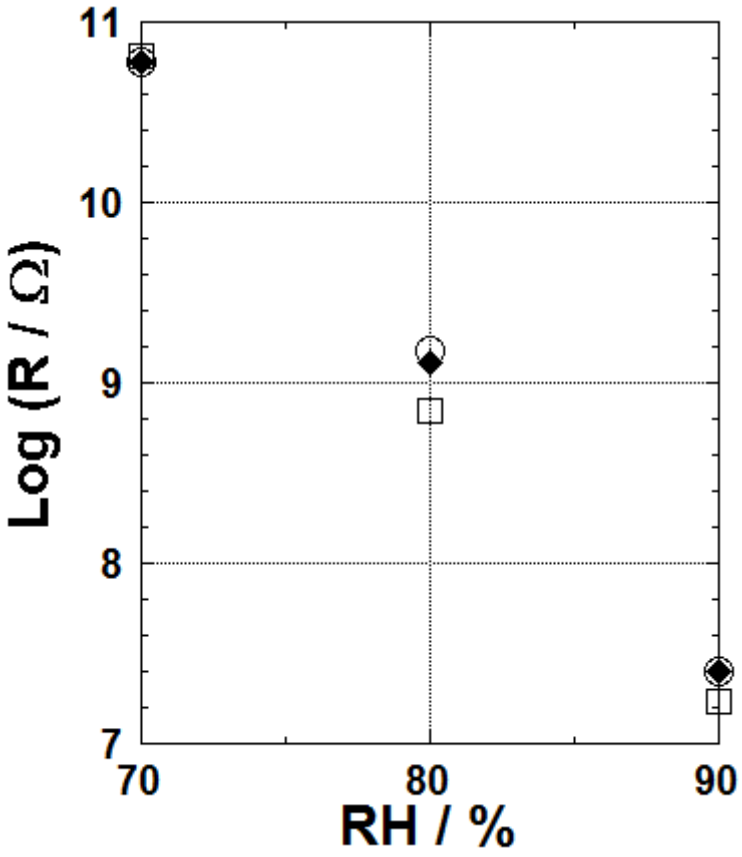

Fig. 6

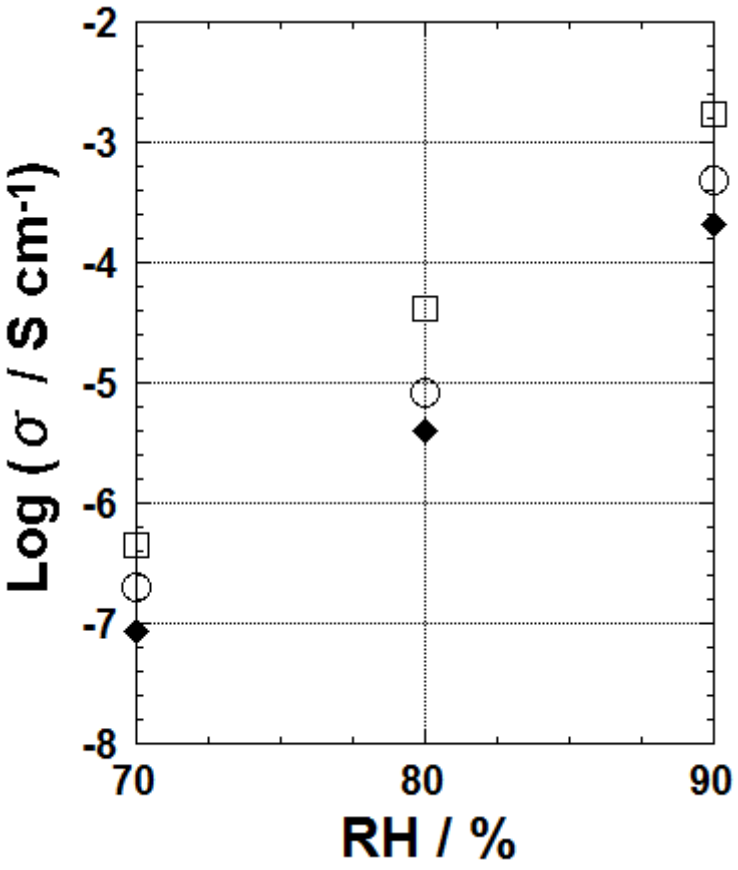

Fig. 7

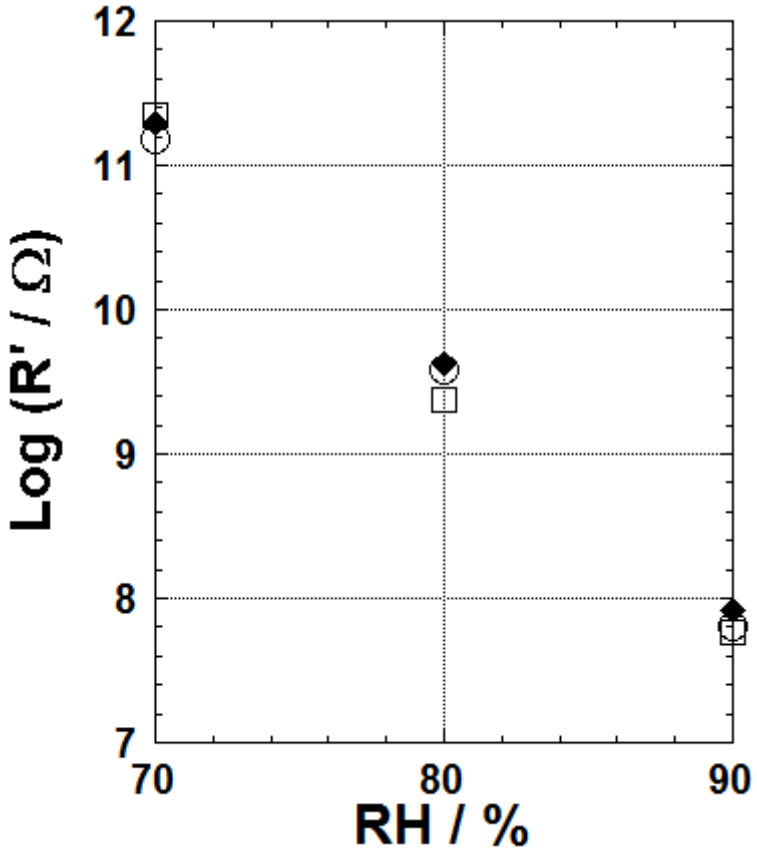

Fig. 8